Biomed Microdevices (2006) 8:291–298
DOI 10.1007/s10544-006-0032-1

Multiscale modeling of protein transport in silicon membrane nanochannels. Part 2. From molecular parameters to a predictive continuum diffusion model

Francesco Amato · Carlo Cosentino · Sabrina Pricl · Marco Ferrone · Maurizio Fermeglia · Mark Ming-Cheng Cheng · Robert Walczak · Mauro Ferrari

Published online: 25 September 2006

Abstract Transport and surface interactions of proteins in nanopore membranes play a key role in many processes of biomedical importance. Although the use of porous materials provides a large surface-to-volume ratio, the efficiency of the operations is often determined by transport behavior, and this is complicated by the fact that transport paths (i.e., the pores) are frequently of molecular dimensions. Under these conditions, a protein diffusion can be slower than predicted from Fick law. The main contribution of this paper is the development of a mathematical model of this phenomenon, whose parameters are computed via molecular modeling, as described Part 1. Our multiscale modeling methodology, validated by using experimental results related to the diffusion of lysozyme molecules, constitutes an "ab initio" recipe, for which no experimental data are needed to predict the protein release, and can be tailored in principle to match any different protein and any different surface, thus filling gap between the nano and the macroscale.

Keywords Multiscale modeling · Protein transport · Non-Fickian release · Nanochannel membranes

F. Amato · C. Cosentino
Department of Experimental and Clinical Medicine, Università degli Studi Magna Graecia, via T. Campanella 115, 88100 Catanzaro, Italy

S. Pricl (✉) · M. Ferrone · M. Fermeglia
Molecular Simulation Engineering (MOSE) Laboratory, Department of Chemical Engineering, University of Trieste, Piazzale Europa 1, 34127 Trieste, Italy
e-mail: sabrina.pricl@dicamp.units.it

M. M.-C. Cheng · R. Walczak
Division of Hematology and Oncology, Department of Internal Medicine, Ohio State University, 1654 Upham Drive,Columbus, Ohio 43210, USA

M. Ferrari
The University of Texas Health Science Center at Houston, 7000 Fannin, Houston, TX 77030, USA

M. Ferrari
The University of Texas M. D. Anderson Cancer Center, 1515 Holcombe Blvd, Houston, TX 77030, USA

M. Ferrari
Rice University, 6100 Main, Houston, TX 77005, USA

1 Introduction

Classical diffusion theory establishes that the movement of solute molecules in a non-homogeneous solution can be predicted, from a macroscopic point of view, by Fick laws. The basic principle is that the flux vector is proportional to the concentration gradient. Fick laws have been successfully applied to predict the diffusion kinetics of molecules through thin semipermeable membranes. Nevertheless, experiments have shown that, as the size of the membrane pores approaches the molecular hydrodynamic radius, unexpected effects, which cause substantial deviations from kinetics predicted by Fick laws, can occur (Martin et al., 2005). Experimental evidence of these unpredicted effects have been also observed in other works (Clark et al., 2000; Auerbach, 2000; Meersmann et al., 2000; Wei et al., 2000; Kukla et al., 1996; Gupta et al., 1996; Hahn et al., 1996), where single file diffusion (SFD) and wall drag effect phenomena have been investigated. In particular, in the case of SFD, the molecular flux is overestimated by Fick law: the kinetics of SFD and Fickian diffusion are different because the molecules in SFD cannot pass each other in nanopores, regardless of the influence of the concentration gradient (Mao and Sinnott, 2000; Nelson

and Auerbach, 1999; MacElroy and Suh, 1997; Nakao, 1994; Aityan and Portnov, 1986; Levitt, 1973).

The case analyzed in Martin et al. (2005) differs from those in other studies (Desai, 2002; Chu and Ferrari, 1998) because the membrane is made up of silicon and fabricated by photolithographic techniques, and the pores are rectangular and nanometric only in one dimension (the other dimensions being in the μm range). The basic principle of diffusion as a mixing process with solutes free to undergo Brownian motion in three dimensions does not apply, since in at least one dimension solute movement within the nanopore is physically constrained by the channel walls. However, unlike the SFD case, the ordering of solute particles imposed by the nanopore geometry is not as strict as true cylindrical pores, but particles could conceivably pass each other laterally. Furthermore, the wall drag effect has been evidenced using plastic micro-sphere moving into microchannels, which could be significantly different from the case of low weight molecules diffusing in nanochannels.

The observable macroscopic effect in Martin et al. consists of a prolonged linear release of several molecules, which eventually switches to an exponential Fick profile (Martin et al., 2005). The diffusion experiments were conducted on silicon microfabricated membranes, consisting of arrays of parallel rectangular channels (see Fig. 1). Anchor points are interposed between the arrays, in order to create structural support. The channels have a width of 45 μm (the distance between two anchor points), and their length is about 4 μm. The microfabrication process allows to precisely tuning the channel height in the range 7–50 nm.

Due to this nanometric features achievable by this technology, nanopore membranes were originally applied to create capsules for the immunoisolation of transplanted islet cells (Desai et al., 1998, 1999). In this setting, the nanopore membrane was designed to serve as the only connection between the reservoir containing the cells and the external medium. The pore height was selected to allow passage of insulin, glucose, oxygen and carbon dioxide-molecules required for proper function of the cell feedback system, while blocking the elements of the immune system which might attack the graft, i.e., the transplanted islet cells. During development of the immunoisolating biocapsule, it was noted that diffusion through nanopore membranes was slower than predicted from Fick law when using smaller pore heights.

Starting from the work of Peskir (2003), the goal of this paper is to develop a model of biomolecular diffusion through nanochannels to provide a reasonable interpretation of the non-Fickian phenomenon. The proposed model recovers the classical (Fick) diffusion laws in the unconstrained case. This is a dynamic model, i.e. it does not consist of a static relation (like a constant gain coefficient) between the flux and other quantities; instead it provides a relation that changes over the phenomenon evolution. The model is implemented in the Matlab-Simulink^{TM} software environment to run virtual experiments by means of pc-based simulations at the continuum scale. The model depends on two molecular parameters which can be computed by using the approach provided in the companion paper (Pricl et al., 2006). Therefore the main contribution of these two papers is that of establishing a methodology which allows *to predict* the kinetics

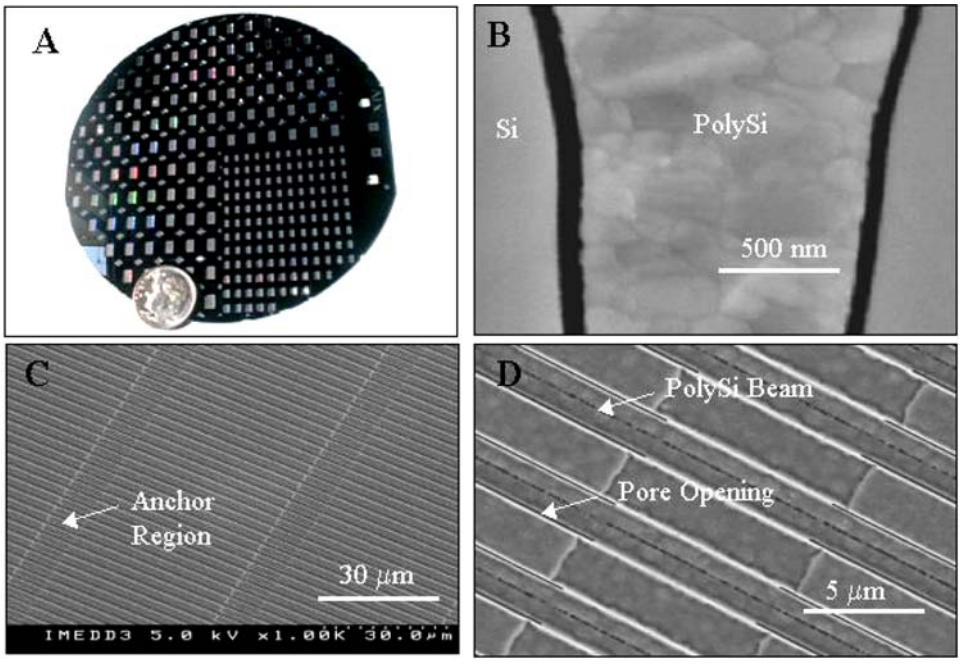

Fig. 1 (A) Appearance of 4 inches silicon wafer showing 120 small and 100 large membrane dies before being cut into individual units. (B) SEM cross-sectional view of membrane with 50 nm pores separated by silicon and poly-silicon material. (C) SEM top view of membrane with pores at 1000× magnification showing 45 μm long pores separated by 10 μm long anchor regions. (D) 6000× top SEM view of membrane showing details of pore and anchor structures

of biomolecular diffusion through membrane nanochannels without requiring, in principle, expensive laboratory experiments. The approach is validated by using the experimental results concerning the diffusion of lysozyme molecules. Simulations reproduce very well the experimental data, thus confirming that the proposed diffusion model can give a reasonable interpretation of the non-Fickian diffusion kinetics.

2 Theoretical background and computational details

When there is a chemical potential gradient in a single-phase fluid mixture, which implies that a concentration gradient is present in the solution, each species will diffuse in the direction of decreasing concentration. The mathematical formula which describes this phenomenon is known as Fick law. It represents a linear relationship between the mass (or molar) flux $\mathbf{J}_\mathrm{A}$ (with respect to the mass average velocity), and the concentration gradient, ∇c_A; for a binary mixture, Fick first law is given by Saatdjian (2000):

$$\mathbf{J}_\mathrm{A} = -D_\mathrm{AB}\nabla c_\mathrm{A} \tag{1}$$

where D_AB is the diffusion coefficient of a solute A in a solvent B. In order to have a good insight of the process, we first apply the classical theory to our specific case-study, but still neglecting the effect of the membrane. Then we will introduce the mathematical description of the membrane effect, so that we can compare this case with the free-diffusion case.

The binary mixture consists of a solvent, e.g. phosphate buffer saline (PBS), and a given solute, which is initially concentrated in a well defined region of the reservoir volume. In order to obtain a suitable model, we require the following hypotheses to hold:

(a) the experimental volume, which contains the drug A, can be divided into two compartments of volume V_1 (the reservoir) and V_2 (the sink), with the respective initial mass concentrations $c^0_{\mathrm{A}1} = c_{\mathrm{A}1}(0)$ and $c^0_{\mathrm{A}2} = c_{\mathrm{A}2}(0)$ $(c^0_{\mathrm{A}1} > c^0_{\mathrm{A}2})$;
(b) the concentration is homogeneous in each compartment and the concentration variation is spatially defined in a thin boundary region of depth L;
(c) given a Cartesian reference system (O, x, y, z), the concentration gradient,∇c_A, has null components along the y and z axes. Therefore the mass flux turns out to be a scalar variable directed along the x axis and denoted by J_A.

Our aim is to calculate the mass flux of drug through a generic surface, of area S, which we assume to be perpendicular to the diffusion path. By a first order approximation (Cosentino et al., 2005) we obtain:

$$J_\mathrm{A}(t) = \left(c^0_{\mathrm{A}1} - c^0_{\mathrm{A}2}\right)\frac{D_\mathrm{AB}}{L}e^{-\lambda_\mathrm{A}\mathrm{t}} \tag{2}$$

where:

$$\lambda_A = \frac{D_{AB}S}{V_1 L}\left(1 + \frac{V_1}{V_2}\right) \tag{3}$$

Therefore in the free diffusion case the release profile is exponential.

At this point we can also calculate the amount of drug A, $Q_A(t)$, which passes from V_1 to V_2 over an arbitrary time interval $[0, t]$, by integrating the mass flux times the area, S, thus obtaining:

$$Q_A(t) = \int SJ_A(t)dt = \left(c^0_{A1} - c^0_{A2}\right)\frac{V_1V_2}{V_1 + V_2}(1 - e^{-\lambda_A t}) \tag{4}$$

Now let us derive the constrained diffusion model. Experimental results show that the release profile remains linear for a certain period, and then it switches to the Fickian exponential trend (Martin et al., 2005). This observation suggests that the classical theory can be still suitable provided that we can devise a more general model capable of explaining the linear release in the first part of the experiment, and recovering the Fickian diffusion kinetics when the concentration drops below a certain threshold. Such model shall also shed some light on the physical mechanisms underlying the non-Fickian behavior observed in the diffusion experiments.

First, consider that classical diffusion theory is based on Einstein relation, which expresses the diffusion coefficient of spherical Brownian particles in a solution as:

$$D_{AB} = \frac{kT}{6\pi r\eta} \tag{5}$$

where k is the Boltzmann constant, T the temperature, r the radius of the solute particles, and η the viscosity coefficient of the liquid.

In order to derive a more general model, one needs to take into account the fact that the mixture does not satisfy the hypothesis of ideal gas law. When the state of Brownian particles in the Einstein argument deviates from the ideal gas law, it assumes the form of the van der Waals equation:

$$\left(p + \frac{a}{\gamma^2}\right)(\gamma - b) = RT \tag{6}$$

where p is the pressure, R is the universal gas constant, and $\gamma = V/n$ is the molar volume, V being the total volume and n the number of moles. It is well known that the constants a and

b have a physical interpretation: The term a/γ^2 represents the additional positive pressure caused by the presence of other solute particles, as a consequence of the long-range attractive forces; the constant b, instead, represents the volume occupied by the gas molecules, so that the term $(\gamma - b)$ represents the effective "free volume".

In the following, we will exploit the work of Peskir (2003) who derived from Eq. (6) the generalized expression for the diffusion coefficient (compare with Eq. (5)):

$$\tilde{D}_{\mathrm{AB}} = \frac{kT}{6\pi r\eta}\left[\frac{1}{(1-b_0\nu)^2} - \frac{2a_0}{kT}\nu\right] \tag{7}$$

where $\nu = \nu(t, x)$ is the average number of Brownian particles at position x at time t, $a_0 = a/N_0^2$, $b_0 = b/N_0$, and N_0 is Avogadro number. Note that the generalized coefficient $\tilde{D}_{\mathrm{AB}}$ recovers the Einstein coefficient D_{AB} when $a = b = 0$.

It is important to note that, according to Eq. (7), the diffusion coefficient is an increasing function of b, and a decreasing function of a. This is intuitively what we could expect, because the value of a is determined by long-range attractive forces, which oppose to particles dispersion, whilst the value of b is related to the short range repulsive forces, which foster particles dispersion. The generalized expression (7) also allows deriving the effect of temperature and pressure variations on the diffusion coefficient: A temperature increase corresponds to a larger diffusion coefficient; conversely, a pressure increase has the opposite effect.

The van der Waals coefficients a and b appearing in Eq. (7) can be computed according to the approach developed in the companion paper (Pricl et al., 2006). The most convenient method (Prausnitz et al., 1986) for linking the van der Waals parameters a and b to the molecular quantities obtained from our molecular dynamics (MD) simulations procedures is provided by the partition function Q. The generalized van der Waals partition function for a pure fluid containing N_m molecules is:

$$Q = \frac{\Lambda^{-3\mathrm{N_m}}}{N_{\mathrm{m}}!}(V_{\mathrm{f}})^{N_{\mathrm{m}}}\left[\exp\left(-\frac{E_0}{2kT}\right)\right]^{N_{\mathrm{m}}} q_{\mathrm{r,v}}^{N_{\mathrm{m}}} \tag{8}$$

where Λ is the de Broglie wavelength, V_{f} is the total free volume, E_0 is the potential field experienced by one molecule due to the attractive forces from all other molecules, and $q_{\mathrm{r,v}}$ is the contribution per molecule from rotational and vibrational degrees of freedom. To a rough first approximation, the free volume and the potential depend only on density. This approximation was used by van der Waals, who for V_{f} assumed the simple relation:

$$V_{\mathrm{f}} = V - \frac{N_{\mathrm{m}}}{N_0}b \tag{9}$$

For E_0, he assumed:

$$E_0 = -\frac{2aN_{\mathrm{m}}}{VN_0^2} \tag{10}$$

From Eqs. (9) and (10) we can easily determine a and b from the other parameters. This will be done later in the case of the lysozyme molecules.

The expression (7) yields the following relation:

$$\frac{\partial\nu}{\partial t} = \left(\frac{kT}{6\pi r\eta}\frac{2b_0}{(1-b_0\nu)^3} - \frac{2a_0}{6\pi r\eta}\right)\left(\frac{\partial\nu}{\partial x}\right)^2 + \left(\frac{kT}{6\pi r\eta}\frac{1}{(1-b_0\nu)^2} - \frac{2a_0}{6\pi r\eta}\nu\right)\frac{\partial^2\nu}{\partial x^2} \tag{11}$$

which is a generalized diffusion law (it recovers Fick second law of diffusion in the case $a = b = 0$) (Saatdjian, 2000).

A finite-element model has been built upon the relation (11) by letting:

$$z_i(t) = \nu(t, x_i), \quad x_i = (i-1)\frac{L}{N}, \quad \mathrm{i} = 1, \ldots, \mathrm{N}+1 \tag{12}$$

Indeed the system described by Eqs. (11) and (12) can be approximated by the following concentrated parameters system:

$$\begin{aligned}
\dot{z}_1(t) &= \frac{\tilde{D}_{\mathrm{AB}}NS}{LV_1}(z_{N+1}(t) - z_N(t)) \\
\dot{z}_k &= \left(\frac{kT}{6\pi r\eta}\frac{2b_0}{(1-b_0z_k)^3} - \frac{2a_0}{6\pi r\eta}\right)\frac{(z_{k+1}-z_{k-1})^2}{4L^2/N^2} \\
&\quad + \left(\frac{kT}{6\pi r\eta}\frac{2b_0}{(1-b_0z_k)^2} - \frac{2a_0}{6\pi r\eta}z_k\right) \\
&\quad \times \frac{(z_{k+1}-2z_k+z_{k-1})}{L^2/N^2}, \quad k = 2, \ldots, N \\
\dot{z}_{N+1}(t) &= -\dot{z}_1(t) = \frac{\tilde{D}_{\mathrm{AB}}NS}{LV_2}(z_N(t) - z_{N+1}(t))
\end{aligned} \tag{13}$$

where the quality of the approximation depends on the number of parameters, N, which corresponds to the number of elementary channel units considered for the discretization. Note that the concentrations in the reservoir and in the sink are represented by the states of the elements at the two extremities of the channel, and the variation of the concentrations at these two points is considered equal and opposite. The discretization of the model allows giving a simple implementation in the Matlab/Simulink™ environment (v. 7.0.1, The MathWorks, Inc., Natick, MA). The main simulation scheme is reported in Fig. 2: the model takes as inputs the rate of variation of the concentrations in the reservoir and in the sink, ν_{A1} and ν_{A2}, and determines the mass fluxes which

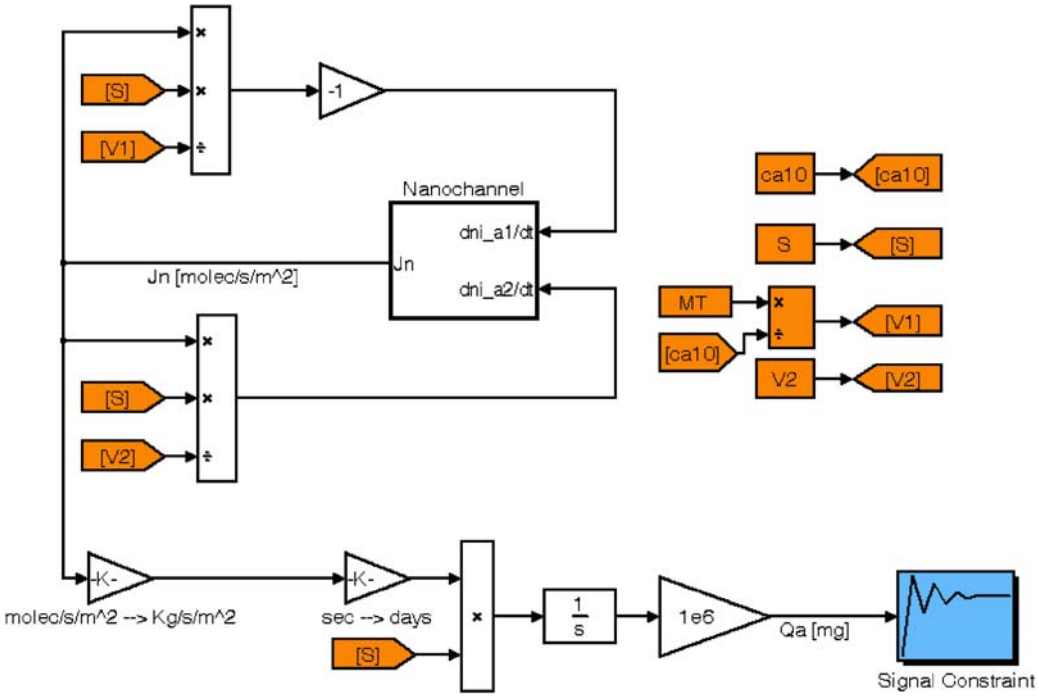

Fig. 2 Simulink model for the computation of the numerical solution of model (13): main view

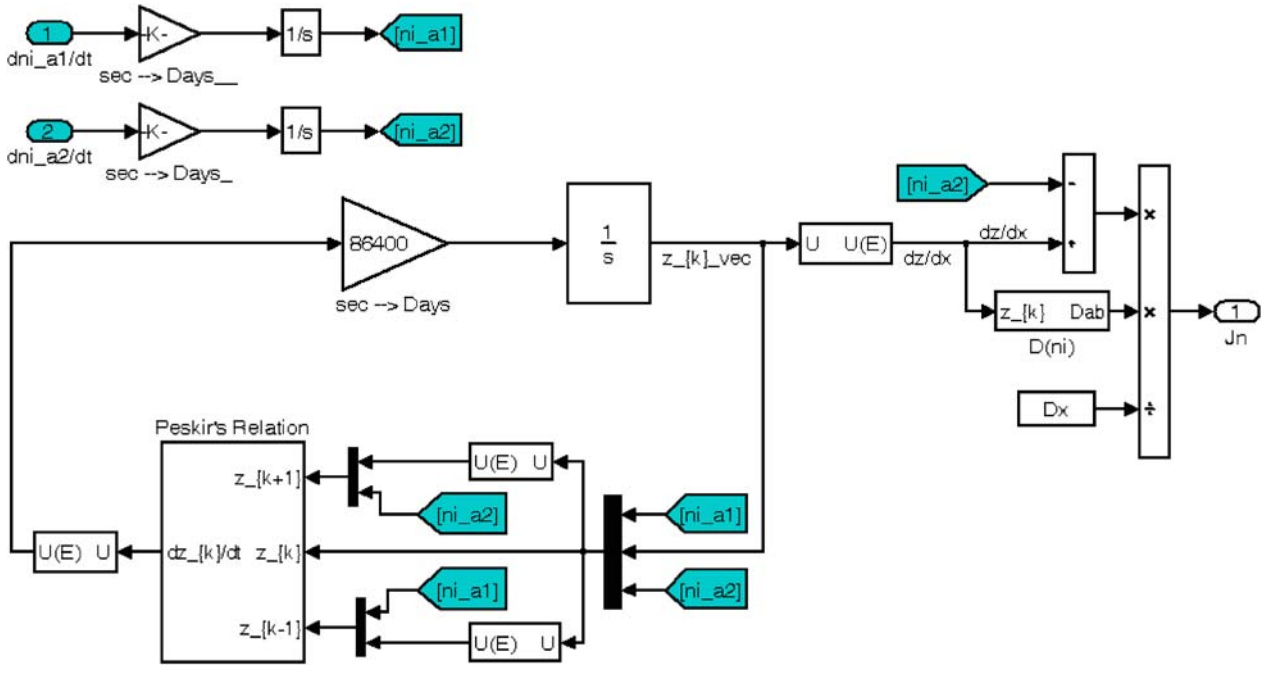

Fig. 3 Simulink model for the computation of the numerical solution of model (12): nanochannel subsystem

enter and exit the channel (which are assumed to be equal and opposite). The flux, in turn, is proportional to the rate of variation of ν_{A1} and ν_{A2}, so the system has the closed-loop structure shown by the scheme.

An important block is the one labeled "signal constraint", which is part of the Simulink response optimization toolbox, and is used to compute the van der Waals coefficients by fitting the experimental data. The nanochannel model is shown in Fig. 3: it implements relation (13), performs the numerical integration of the zk variables, and computes the mass flux at the edge of the channel communicating with the sink.

3 Results and discussion

According to our multiscale simulation recipe, we exploit the model described in the previous section to interpret some experimental results concerning the diffusion of lysozyme (Martin et al., 2005). In this case, we simply equated the parameter b to the lysozyme molar volume. The parameter E_0 was calculated, according to its definition (10), as the potential energy of interaction exerted on the free lysozyme molecule by the bound one at minimum. In details, since the van der Waals molecular volume of lysozyme $V_{\mathrm{vdW,HEWL}} = 16651$ Å (Pricl et al., 2006), the parameter b is equal to:

$$b = V_{\mathrm{vdW,HEWL}} \times N_0 = 0.0100\,\mathrm{m}^3 \tag{14}$$

The value of the interaction parameter a is then calculated by recasting Eq. (10) as:

$$a = -\frac{E_0 V N_{\mathrm{A}}^2}{2N_{\mathrm{m}}} = 6.95 \times 10^3\,\mathrm{Pa\,m}^6 \tag{15}$$

in which the number N_m of interacting molecule is 2 (i.e., the bound and free HEWL molecules), and the total volume is set equal to the volume of the simulation cell: $V = 4.91 \times 10^{-25}$ m^3. The value of E_0 is obtained from the minimum of the potential energy of interaction curve between the free and bound HEWL molecules, $E_{min} = -93.93$ kJ/mol, as $E_0 = E_{min}/N_0 = -1.56 \times 10^{-19}$ J/molecule (Pricl et al., 2006).

The release profile obtained for lysozyme (14 kDa) by our model is shown in Fig. 4 together with the experimental data and the profile estimated by Fick law. The initial concentration is 5 mg/ml and the membrane channel height 13 nm. The solvent used is PBS. Although lysozyme release data have not been shown in the paper by Martin et al. (2005), the reader can refer to materials and methods reported there, which are similar to the ones used for the lysozyme diffusion experiments.

From Fig. 4 it is evident how the diffusion profile estimated by Fick law is completely different from the experimental one. Moreover it is important to note that, even if the experimental parameter values were varied, Fick law could not explain the experimental data, because the initial part of the release curve is almost linear, which is not in agreement with classical diffusion theory. The experimental behavior, instead, agrees with the proposed nanochannel diffusion model, which is coherent with the data before and after the "switch" to the Fickian behavior. In Fig. 4 it is also reported the diffusion profile of the model obtained by selecting the parameters a and b which better fit, according to a mean square error policy, the experimental data. It is worth noting that the model obtained by selecting the parameters according to Eqs. (14) and (15) (which does not need the information coming from the experimental results) works even better than the model derived from the data fitting for a period covering the first 20–25 days (actually our model describes almost perfectly the experimental data for the first 20 days). Moreover, the last part of the experimental curve is not completely reliable, due to the offset caused by the experimental errors which cumulate day after day; this could explain the discrepancies between the proposed model and

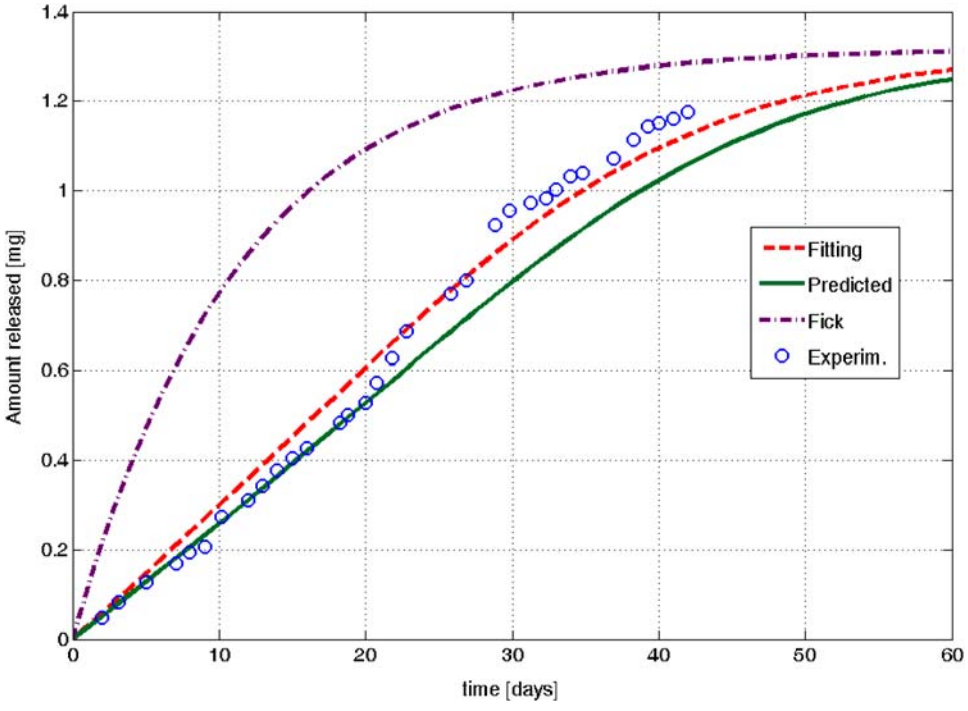

Fig. 4 *In vitro* lysozyme diffusion through nanopore membrane (13 nm pore height): Fick law prediction (- ·), model based simulation with parameters derived by fitting (--), model based simulation with parameters derived by molecular dynamics simulation (-), experimental data (o)

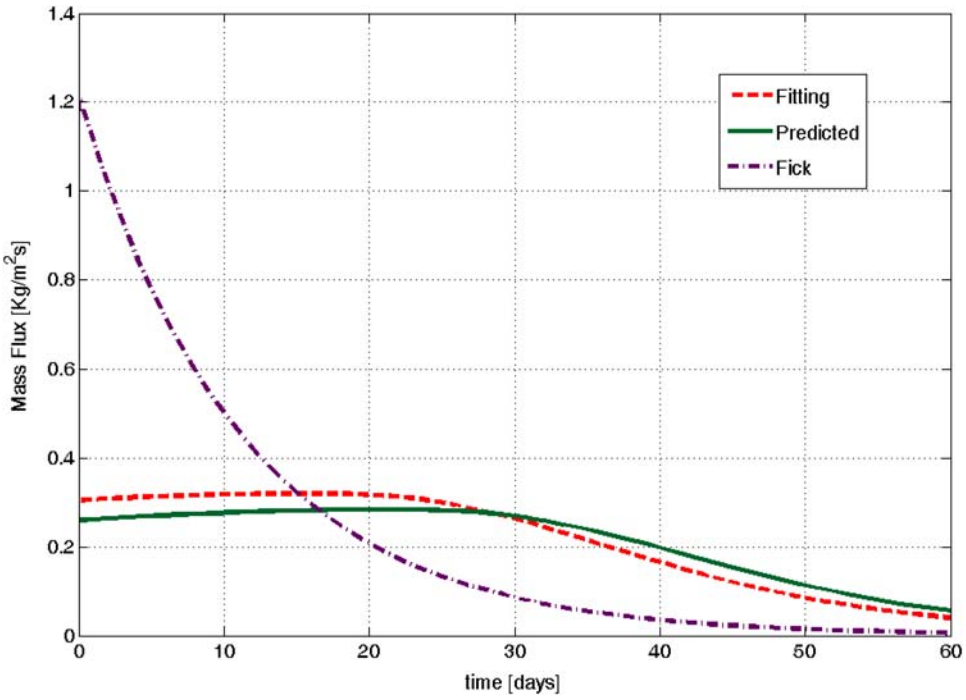

Fig. 5 Lysozyme mass flux through a 13 nm pore height membrane: Fick law prediction (- ·), model based simulation with parameters derived by fitting (--), model based simulation with parameters derived by molecular dynamics simulation (-)

the data after day 25. In Fig. 5 the mass flux predicted by our model is reported together with the mass flux estimated by Fick law and the mass flux obtained by the fitting model. The results obtained can be used to predict the diffusion of different molecules, given the channel height, and suggest that nanopore membranes can be engineered to control diffusion rates and kinetic order by "fine-tuning" channel height in relation to the size of solutes. Moreover, when the proper balance is struck, zero-order diffusion kinetics is possible. Implantable zero-order output devices are useful to deliver drugs which are not orally bio-available, particularly in clinical settings, where maintenance of a steady state level in the blood stream for long periods is desirable. On the basis of these results we can also conclude that the total molecular flux through the membrane can be controlled by varying the porosity and the total porous area, whereas the diffusion kinetics can be controlled by changing the channel height. Whether a consequence of a SFD-like phenomenon or drag effects (or a combination of both), the nanopore membrane used here is rate-limiting and, if properly tuned, restricts solute diffusion to a point that flux rate across the membrane is entirely independent of the concentration gradient.

4 Conclusions

Understanding the mechanism of diffusion through nanochannels is important not only from a theoretical perspective, but also in view of the potential applications of nanopore silicon membranes. The release rate has been shown to be constant for a long period, under suitable choice of the experimental parameters (initial concentration, channel height and size of solutes); this property can be exploited in clinical medicine for prolonged and constant administration of drugs. In this case it is of paramount importance to have a quantitative method for the device tuning and the prediction of the amount of drug released in the patient within a certain time period. Furthermore, the model could also be used as a tool for quality control of the membranes fabrication process, which, at present, represents a difficult task to perform in a non-destructive way.

In conclusion, in these two paper series we have formulated a multiscale simulation approach to the biomacromolecule diffusion in nanochannels, based on computer simulations spanning from the atomic world to the continuum dimension. Long regarded as a purely mathematical subject, molecular multiscale modeling can now be considered as most relevant for its physical significance. Molecular engineering is indeed entering a new era, characterized by an unprecedented control over chemical reaction, as well as product molecular architecture, conformations and morphology. It is entering an era of molecular processing and manufacturing, in which singe-molecule experiments are becoming routine, and complex miniature processes are beginning to be commercialized for a number of different applications. These experiments and processes not only benefit from modeling but, in some cases, must be interpreted or implemented through a concerted modeling effort. Molecular multiscale modeling thus provides a sort of unifying set of principles to understand and interpret the behavior of seemingly different

systems on common grounds. It provides a common language that enables practitioners of molecular engineering to approach problems in areas as diverse as, for instance, chemical sensing, microfluidics, genetics, and last but not least, nanomechanical microdevices such as that described in Part II of this series of papers. Without this language, it would be difficult to tackle such problems on a rational basis.

Acknowledgments MCC, RW and MF are grateful to the National Cancer Institute and BRTT of the State of Ohio for their support of this work. This project has been partially funded by National Cancer Institute, National Institute of Health under Contract No. NO1-CO-12400. SP, MF and MF acknowledge the generous financial support from the Italian Association for Cancer Research (AIRC), grant 2955.

References

S.K. Aityan and V.I. Portnov, Gen. Physiol. Biophys. **5**, 351 (1986).
S.M. Auerbach, Intl. Rev. Phys. Chem. **19**, 155 (2000).
W.H. Chu and M. Ferrari, Micromachined Capsules Having Porous Membranes and Bulk Supports, US Patent No. 5, 770,076 (1998).
L.A. Clark, G.T. Ye, and R.Q. Snurr, Phys. Rev. Lett. **84**, 2893 (2000).
C. Cosentino, F. Amato, R. Walczak, A. Boiarski, and M. Ferrari, J. Phys. Chem. B **109**, 7358 (2005).
T.A. Desai, Exp. Op. Biol. Ther. **2**, 633 (2002).
T.A. Desai, W.H. Chu, J.K. Tu, G.M. Beattie, A. Hayek, and Ferrari, Biotechnol. Bioeng. **57**, 118 (1998).
T.A. Desai, D. Hansford, and M. Ferrari, J. Membrane Sci. **159**, 221 (1999).
V. Gupta, S.S. Nivarthi, D. Keffer, A.V. McCormick, and H.T. Davis, Science **274**, 164 (1996).
K. Hahn, J. Karger, and V. Kukla, Physical Rev. Lett. **76**, 2762 (1996).
V. Kukla, J. Kornatowski, D. Demuth, I. Girnus, H. Pfeifer, L.V.C. Rees, S. Schunk, K.K. Unger, and J. Karger, Science **272**, 702 (1996).
D.G. Levitt, Phys. Rev. A **8**, 3050 (1973).
J.M.D. MacElroy and S.H. Suh, J. Chem. Phys. **106**, 8595 (1997).
Z. Mao and S.B. Sinnott, J. Phys. Chem. B **104**, 4618 (2000).
F. Martin, R. Walczak, A. Boiarski, M. Cohen, T. West, C. Cosentino, and M. Ferrari, J. Controlled Rel. **102**, 123 (2005).
T. Meersmann, J.W. Logan, R. Simonutti, S. Caldarelli, A. Comotti, P. Sozzani, L.G. Kaiser, and A. Pines, J. Phys. Chem. A **104**, 11665 (2000).
S. Nakao, J. Membrane Sci. **96**, 131 (1994).
P. Nelson and S. Auerbach, J. Chem. Phys. **110**, 9235 (1999).
G. Peskir, Stoch. Models **19**, 383 (2003).
J.M. Prausnitz, R.N. Lichtenthaler, and E.D. de Azevedo, E.D. Molecular Thermodynamics of Fluid-Phase Equilibria (Prentice Hall Inc., Englewood Cliffs, N.J., 1986).
S. Pricl, M. Ferrone, M. Fermeglia, F. Amato, C. Cosentino, M.M.-C. Cheng, and M. Ferrari, Biomed. Microdev. this issue (2006).
E. Saatdjian, Transport Phenomena Equations and Numerical Solutions (Wiley & Sons, New York, 2000).
Q. Wei, C. Bechinger, and P. Leiderer, Science **287**, 625 (2000).